

# Hydraulic Fracturing and Production Optimization in Eagle Ford Shale Using Coupled Geomechanics and Fluid Flow Model

Theerapat Suppachoknirun<sup>1,2</sup> · Azra N. Tutuncu<sup>2</sup>

Received: 16 July 2017 / Accepted: 30 October 2017 / Published online: 10 November 2017  
© Springer-Verlag GmbH Austria 2017

**Abstract** With increasing production from shale gas and tight oil reservoirs, horizontal drilling and multistage hydraulic fracturing processes have become a routine procedure in unconventional field development efforts. Natural fractures play a critical role in hydraulic fracture growth, subsequently affecting stimulated reservoir volume and the production efficiency. Moreover, the existing fractures can also contribute to the pressure-dependent fluid leak-off during the operations. Hence, a reliable identification of the discrete fracture network covering the zone of interest prior to the hydraulic fracturing design needs to be incorporated into the hydraulic fracturing and reservoir simulations for realistic representation of the in situ reservoir conditions. In this research study, an integrated 3-D fracture and fluid flow model have been developed using a new approach to simulate the fluid flow and deliver reliable production forecasting in naturally fractured and hydraulically stimulated tight reservoirs. The model was created with three key modules. A complex 3-D discrete fracture network model introduces realistic natural fracture geometry with the associated fractured reservoir characteristics. A hydraulic fracturing model is created utilizing the discrete fracture network for simulation of the hydraulic fracture and flow in the complex discrete fracture network. Finally, a reservoir model with the production grid system is used allowing the user to efficiently perform the fluid flow simulation in tight formations with complex fracture networks. The complex

discrete natural fracture model, the integrated discrete fracture model for the hydraulic fracturing, the fluid flow model, and the input dataset have been validated against microseismic fracture mapping and commingled production data obtained from a well pad with three horizontal production wells located in the Eagle Ford oil window in south Texas. Two other fracturing geometries were also evaluated to optimize the cumulative production and for the three wells individually. Significant reduction in the production rate in early production times is anticipated in tight reservoirs regardless of the fracturing techniques implemented. The simulations conducted using the alternating fracturing technique led to more oil production than when zipper fracturing was used for a 20-year production period. Yet, due to the decline experienced, the differences in cumulative production get smaller, and the alternating fracturing is not practically implementable while field application of zipper fracturing technique is more practical and widely used.

**Keywords** Discrete fracture network · Natural fractures · 3-D complex DFN · Eagle Ford shale · Hydraulic fracture geometry · Zipper fracture · Alternating fracture · Consecutive fracture · Reservoir simulation · Production profile

## List of symbols

$E$	Young's modulus
$E'$	Plane-strain Young's modulus
$H_f$	Fracture height
$H_{fl}$	Local height of the fracture under consideration
$h_L$	Leak-off height
$K_{Ic}$	Formation fracture toughness in opening mode
$K_{Iu}$	Stress intensity factors at the upper tip, considering tensile failure (mode I)

✉ Azra N. Tutuncu  
atutuncu@mines.edu

<sup>1</sup> Present Address: PTT Exploration and Production Plc., Bangkok, Thailand

<sup>2</sup> Colorado School of Mines, 1500 Illinois Street, Golden, CO 80401, USA

$K_{II}$	Stress intensity factors at the lower tip, considering tensile failure (mode I)
$L(t)$	Fracture length as a function of time
$n$	Power-law fluid index
$n_f$	Fracturing stage number
$p_b$	Bubble point pressure
$p_{bd}$	Breakdown pressure in hydraulic fracturing operation
$p_c$	Fracture closure pressure
$p_{ob}$	Overburden pressure
$p_p$	Pore pressure
$\Delta p_{net}$	Different between closure pressure and the pressure in fracture
$Q(t)$	Pump rate or injection rate as a function of time,
$q_L$	Leak-off rate per unit length
$q_l$	Fluid leak-off rate
$T_0$	Tensile strength
$u$	Sneddon's displacement
$u_L$	Leak-off velocity
$w_0$	Maximum fracture width
$w$	Average fracture width
$x_F$	Fracture half-length
$\alpha$	Biot coefficient in an isotropic formation
$\alpha_h$	Biot coefficient in minimum horizontal direction
$\alpha_v$	Vertical Biot coefficient
$\rho_f$	Fluid density
$\sigma_{  }$	Stress that is parallel to the fracture face
$\sigma_{\perp}$	Stress that is perpendicular to fracture face
$\sigma_{H,max}$	Maximum horizontal stress
$\sigma_{h,min}$	Minimum horizontal stress
$\sigma_n$	Normal stress
$\sigma_{ob}$	Overburden stress
$\sigma_r$	Radial stress
$\sigma_s$	Shear stress
$\sigma_{tect}$	Tectonic-induced stress
$\sigma_{tip}$	In situ stress at the top tip
$\sigma_v$	Vertical stress
$\sigma_{\beta y}$	The normal stress acting on the fracture interface
$\sigma_{\theta}$	Tangential stress
$\bar{\tau}$	Shear tensor
$\tau_{\beta}$	The shear stress acting on the fracture interface
$\tau$	Time at fluid start to leak out of the fracture at the particular location
$\mu$	Fluid viscosity

## 1 Introduction

The advent of coupling horizontal drilling and multistage fracturing has made it possible to produce from shale gas and tight oil reservoirs making these complex reservoirs key contributors to the oil and gas production in the USA in the past few years. The significant advancements that made

possible by drilling the wells with an extension of several kilometers laterally into the reservoir and then fracturing them throughout the full length of the horizontal sections provide an opportunity to manage unconventional oil and gas development in a manner that greatly increases the production. Yet, the early production rapidly declines, requiring new wells to maintain the production in these unconventional tight reservoirs. Better understanding and coupling the formation of geomechanical characteristics with fluid transport will promote natural and induced fracture interactions and mitigate in situ stress alterations taking place during hydraulic fracturing. The coupled geomechanics and fluid flow modeling will also help to inhibit unfavorable fracture propagation and identify suitable fracturing geometries to allow optimization of production in these reservoirs.

The complex fracture network introduced through hydraulic fracturing in naturally fractured tight formations is not truly captured in traditional black oil reservoir simulators. A network of planar fractures is placed at predetermined locations in these models while the propagation of the hydraulic fractures is significantly altered by the presence of natural fractures. The density and distribution of these natural fractures often differ from reservoir to reservoir and even from one section to another within a reservoir based on the depositional and tectonic histories during the geological times up to the present day. When the natural fractures are not included in the hydraulic fracturing model, the combined fracture network and the associated production forecasting simulation using the inaccurate fracture network used as input into reservoir simulator, the production forecasting will be obsolete.

The consideration of the fracture propagation behavior including the interactions taking place between the natural fractures and approaching hydraulically induced fractures, the effects of formation rock and native fluid properties on the growth of the fracture, the stress shadow and associated in situ stress alterations, and fluid and proppant transport selection enhance accurate and realistic representation of the fracture network geometry and associated production forecasting as presented in this study.

A complex fracture network model combining the natural fracture network enhanced by the hydraulically induced fractures capturing the real subsurface characteristics is essential for the subsequent analyses for realistic evaluation of production potential.

An increase in oil and gas production can be accomplished with a suitable hydraulic fracturing introducing higher connectivity as a result of the combined discrete fracture network. When the fracture conductivity created using solely the planar fractures without including the natural fractures and other complexities, the outcome will not be a realistic representation of the reservoir conditions. The in situ formation stress alterations as a result of the multistage hydraulic fracturing

within the stress shadow region will also cause redirection of the hydraulic fractures, especially when a horizontal well is fractured from toe to heel in consecutive order as shown in Fig. 1 (Tutuncu 2017; Suppachoknirun and Tutuncu 2016). Other hydraulic fracturing geometries with specific staging placement with respect to two or three parallel horizontal sections have been implemented to provide more options toward optimization of the stimulated reservoir volume (SRV) and optimizing production. Zipper fracturing and alternating techniques have been developed for this purpose in order to increase the fracture complexity and associated production.

Horizontal wells in shale reservoirs are typically fractured in several stages. Consecutive fracturing is when the fracturing is started at the toe of the horizontal well and move toward the heel of the well (Fig. 1a). As the use of multi-stage fracturing has become routine, new processes have been implemented to enhance the stimulated reservoir volume by creating a more complex fracture network between the stages in parallel horizontal wells. Alternate fracturing is used to take advantage of the stress shadow effect (Tutuncu 2017). After the first fracture at the toe is placed, the second fracture is performed at the location where the original third fracture would be planned (Fig. 1b). Then, the third fracture is placed between the two fractures to decrease the spacing between the fractures and to introduce more complex fracture networks in this highly altered stress region. Zipper fracturing (Fig. 1c) is the most favorable pattern used in shale gas and tight oil hydraulic fracturing. Two or three parallel horizontal wells are stimulated from toe to heel concurrently forcing fracture propagation perpendicular to the main fracture (Waters et al. 2009; Rafiee et al. 2012). Shifting the distance in one of the laterals to create further staggered fractures has become a preferred technique entitled “modified zipper fracturing” and was also extended to more than two parallel wells as discussed by Roussel and Sharma (2011).

In this study, the development of a discrete fracture network (DFN) model, its validation and utilization for production predictions for an Eagle Ford well pad have been presented using a reservoir simulation model. Various hydraulic fracturing patterns including alternating, consecutive and zipper fracturing techniques have been evaluated in the presence of native fractures to define optimized fracture geometry. The recommendations provided from the study provide the operators guidance for optimized production during the selection of the field development plan decision making.

## 2 Study Area and Reservoir Formation Characteristics

The Eagle Ford formation, an Upper Cretaceous deposit, formed during a sea-level transgression in an isolated

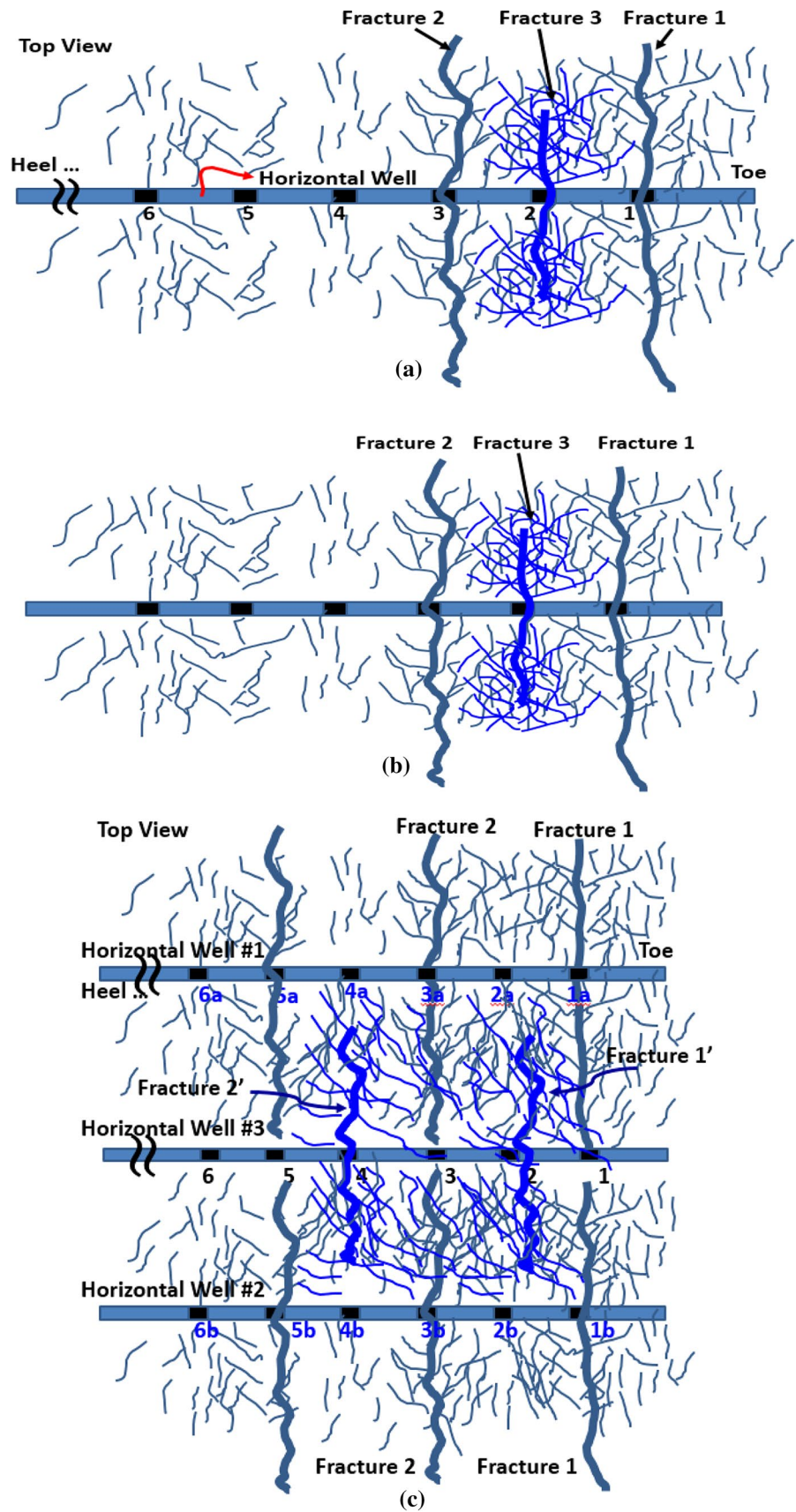
carbonate platform surrounded by siliciclastics (Donovan and Staerker 2010) overlain by Austin Chalk and lying above Buda limestone. It is named after the town of Eagle Ford, Texas, located in the Dallas—Fort Worth metropolitan area outcrop and extends from the northeast to southwest across the State of Texas in the USA with gas, condensate, and oil window, spread along its over 50-mile-wide, 650-km-long extent (Robinson 1997). The formation depth and thickness vary with the constraints imposed by regional tectonic features like the Maverick Basin, San Marcos Arch, Stuart City and Sligo shelf Margin, and the East Texas Basin (US EIA 2014) ranging from 450 meters to approximately 4250 m down-dipping toward the Edwards and Sligo Shelf edges with thicknesses ranging between 15 and 90 m. (Martin et al. 2011).

The Eagle Ford formation has very low permeability with varying mineral and organic compositions as shown in Fig. 2 for a cross-sectional representation between two wells where UNGI-preserved cores and field data analysis are conducted (Tutuncu 2015). The well on the left is in La Salle County in the southwest, while the one on the right is in Gonzales County in the northeast of the field; both are in the oil window section. The presence of high organic composition and high clay content reduces static moduli as well as the strength of the formation and introduces additional anisotropy as presented in Fig. 3.

High pore pressure is a characteristic observed in the lower Eagle Ford facies due to the hydrocarbon generation and associated volumetric expansion. Fine laminations and preexisting natural fractures have also been a common feature in both the upper and lower Eagle Ford causing mechanical anisotropy, inducing the directional-dependent behavior of the formation elastic properties along with anisotropic tensile failure behavior. Fracture models using elastic approaches predict fractures along the loading direction. However, most measurements, particularly the specimens containing natural fractures, created fractures away from the central plane, which is not captured in elastic models. In recent years, new fracturing models have been developed to incorporate some of the complexities in stimulating naturally fractured formations. The interaction between the hydraulic fracture and natural fractures could cause fluid loss into the natural fracture, dilation of the natural fracture due to shear or tension in addition to potential branching or alteration of the hydraulic fracture path as illustrated in Fig. 4.

Tensile failure observed in the Brazilian tests is complex due to the existence of natural fractures and heterogeneity. Mokhtari et al. (2014) presented Brazilian failure measurements that showed the anisotropic tensile strength in Eagle Ford due to lamination. They also tested Niobrara shale specimens containing a calcite-filled fracture to illustrate that natural fracture orientation is critical for the interaction of the hydraulic and natural fractures and affects the

**Fig. 1** Fracture placement in **a** consecutive fracturing at a horizontal well, **b** alternate fracturing in a horizontal well, and **c** zipper fracturing in three-well pattern (Tutuncu 2017)



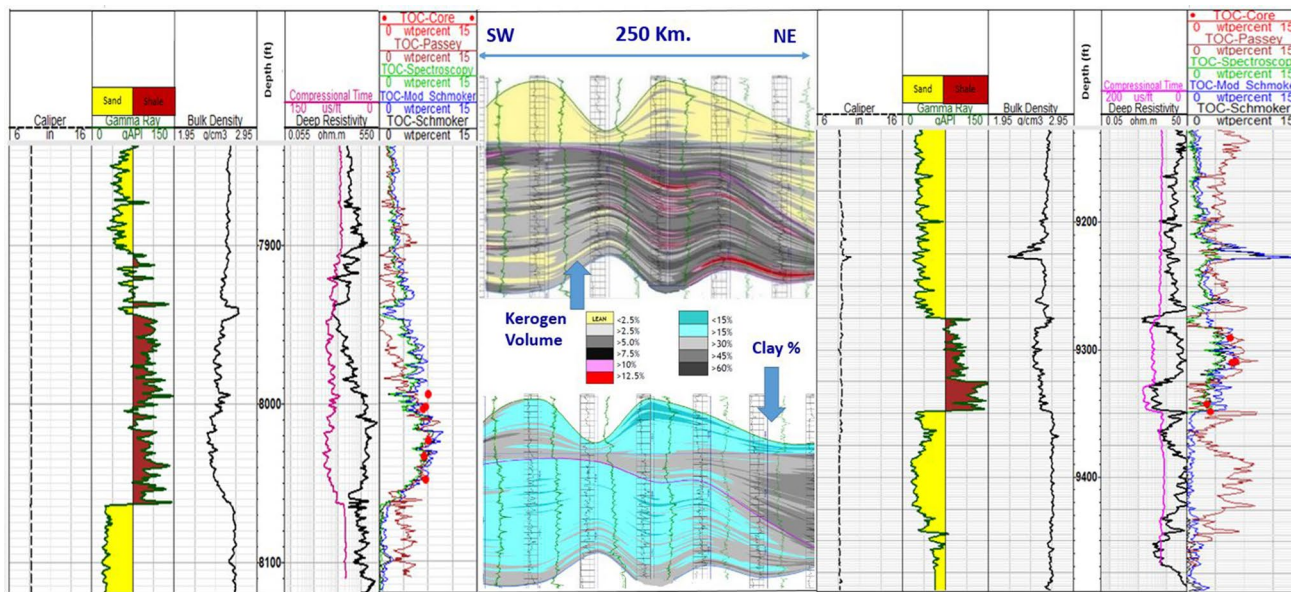
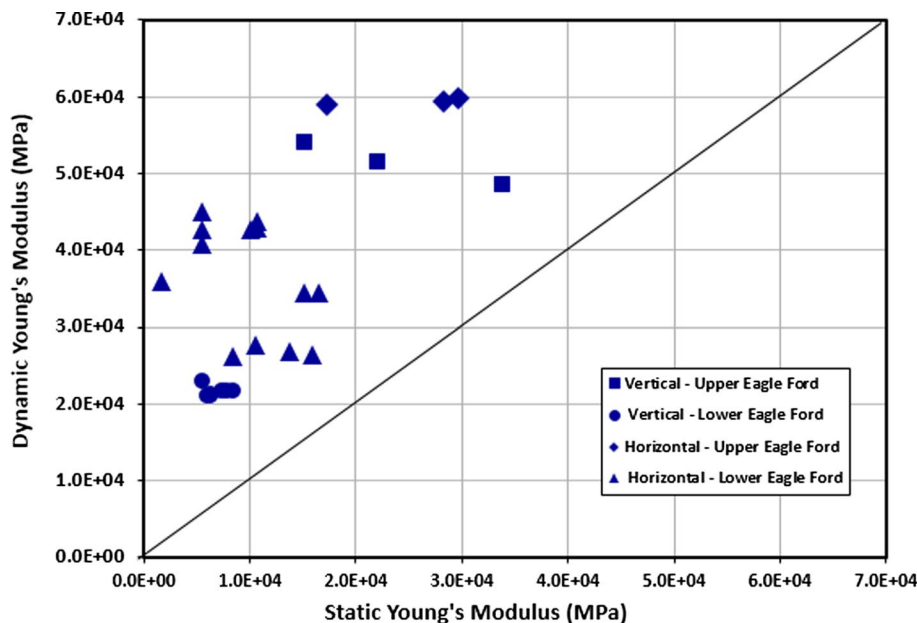


**Fig. 2** Cross section starting at La Salle and ending in Gonzales counties for the Eagle Ford formation utilizing the two UNGI core wells studied 250 km. apart as well as several other wells obtained from Drilling Info database between the two core wells. Note the dis-

tinct variation of the TOC and clay content across the field. TOC values have been measured from cores and also using velocity-resistivity log differences utilizing several methodologies and calibrated with the TOC from the core measurements (modified after Tutuncu 2015)

**Fig. 3** Dynamic–Static Moduli differences measured in upper and lower Eagle Ford preserved intact core samples from two wells approximately 250 km apart (Tutuncu et al. 2016)



induced fracture direction. In laminated Eagle Ford specimens, induced fracture is observed to deviate toward the lamination when lamination is parallel to the applied stress while the failure occurred away from the lamination in the lamination perpendicular to the applied stress as shown in Fig. 5a. Similar results were obtained when calcite-filled fractured Niobrara specimens were tested (Fig. 5b). The associated tensile strength is low when the weakness plane is parallel to applied stress.

Through detailed geomechanics measurements and nanoscale imaging analysis from preserved Eagle Ford cores, Padin et al. (2014) and Padin et al. (2016) proposed that horizontal microfractures initiate in the abnormal stress regime in the lower Eagle Ford, where the vertical stress is not the maximum principal stress resulting in the propagation of these fractures parallel to the interfaces of the bedding planes due to the lower tensile strength in the interfaces.

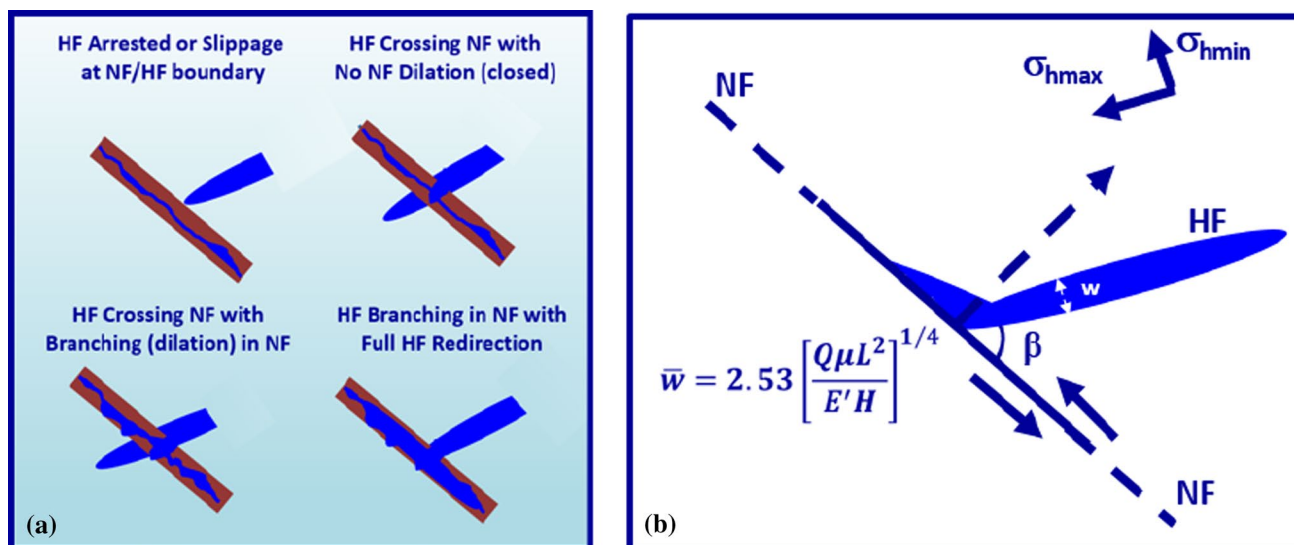


**Fig. 4** Four possible scenarios of the interaction between a natural fracture (NF) and an approaching hydraulic fracture (HF). **a** (1) HF arrests or slippage takes place at the NF/HF boundary, (2) HF crosses NF with no dilation at the NF leaving NF closed, (3) HF crosses the NF causing dilation of the NF and branching, (4) HF branches at the

NF redirecting along the NF. **b** The average width of the hydraulic fracture ( $w$ ) is calculated in all four cases based on the stiffness of the fracture (plane-strain Young's Modulus  $E'$ ), length ( $L$ ) and height ( $H$ ) of the fracture, viscosity of the fluid in the fracture  $\mu$  and the fluid leak-off rate  $Q$

Three multiple horizontal wells located in the oil window of Eagle Ford formation were used for the optimization study. The well-pad location and the details for the three horizontal well spacings are presented in Figs. 6 and 7, respectively. Lateral sections of the wells T-1, T-3, and T-5 are within the lower Eagle Ford formation at approximately 3292 m. depth. The wells were completed using plug-and-perf completion and were hydraulically fractured using a zipper fracturing pattern in three-well layout for 41 stages in total. The log data were used for one of the parameters used as input data either directly obtained from the vertical section of the well or generated utilizing nearby wells with similar stratigraphy for verification. The geomechanical, acoustic, and permeability experimental data collected at the UNGI-coupled geomechanics laboratory from the preserved cores in the production interval in a well in La Salle County were also used as part of the input data in the model.

It is important to properly consider fracture propagation, which is based on the properties and characteristics of the formation to accurately represent the complex fracture network resulting from hydraulic fracturing operations in a naturally fractured formation. In this study, the development of the DFN has taken into account four significant aspects, namely the hydraulic fracture propagation mechanics, the fluid and proppant transport inside the fracture, the stress shadow effect created by prior fracture stages, and the interactions between an approaching hydraulically induced fracture and the natural fracture during the hydraulic fracturing operation. All of these have been considered based on the

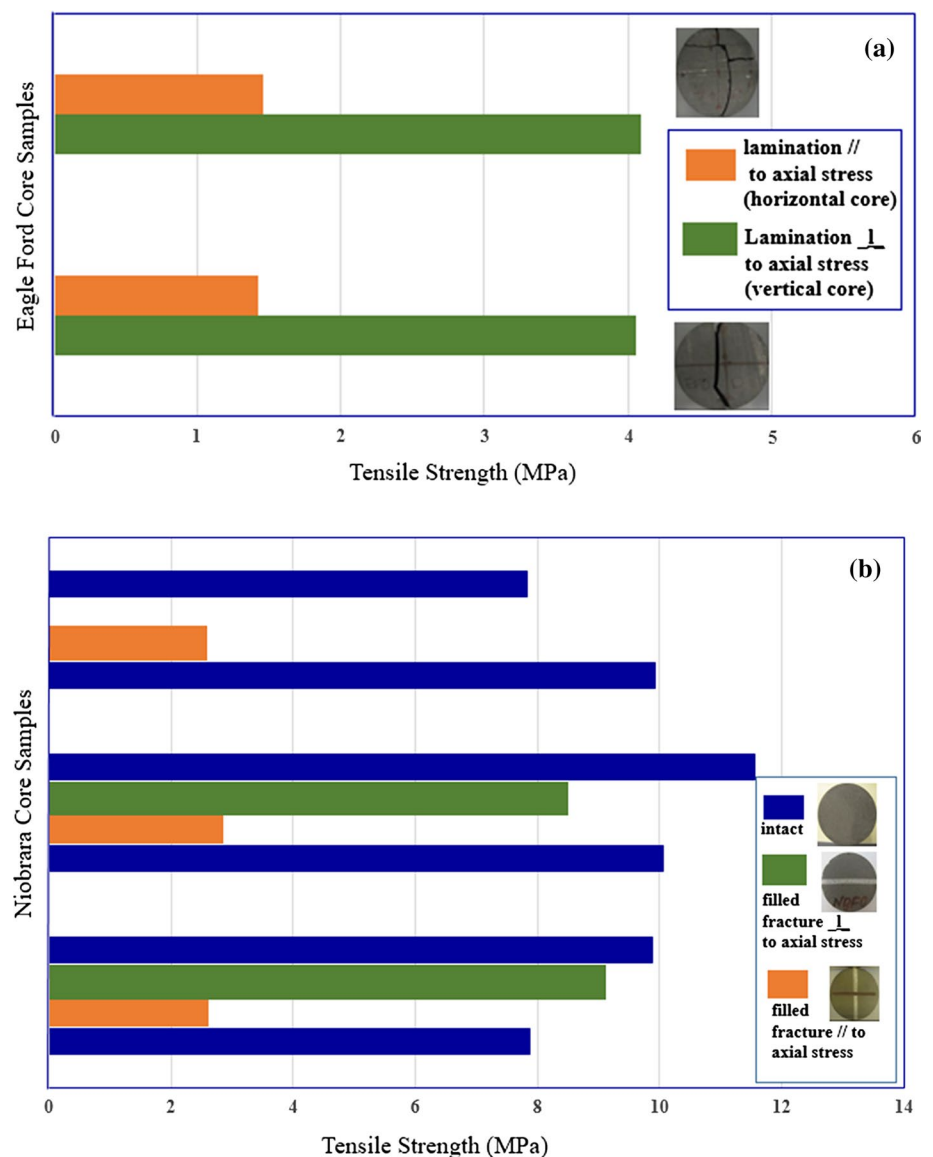
reservoir properties obtained from the measurements of geomechanical properties, permeability, ultrasonic velocity, and resistivity under undrained conditions, well logging data obtained in the core wells, and characterization of the preexisting fractures in the formation being studied utilizing geological studies, imaging and other logs, fracturing and microseismic data from the wells and coupling these datasets in the model.

### 3 Coupled Geomechanics and Flow Model for Reservoir Characterization, Hydraulic Fracturing, and Production in Tight Formations

Natural fractures in tight formations, particularly in shale reservoirs, are important to consider since they play a critical role influencing the completion and stimulation effectiveness through the varying properties of the complex fracture network induced during the hydraulic fracturing operations. These natural fractures subsequently affect the stimulated reservoir volume and need to be characterized prior to hydraulic fracturing design to maximize the stimulation benefit for optimizing production.

A consistent characterization of the discrete fracture network (DFN) covering the zones of interest is essential for a more reliable production forecast. Moreover, the DFN can be used to determine the efficiency of the hydraulic fracturing, damage mechanisms involved and potential production enhancement solutions for future field development efforts.

**Fig. 5 a** Tensile strength reduction and deviation of the fracture propagation from the lamination was observed in Eagle Ford specimens. **b** Tensile strength of intact and calcite-filled fractured Niobrara shale specimens. When the filled fracture is perpendicular to the axial stress, the tensile strength is significantly lower than when the filled fracture is parallel to the axial stress. Moreover, the fracture propagation is not always along the filled fracture direction. Measurements have been taken using Brazilian tensile tests at the UNGI-coupled geomechanics laboratory



Yet, creation of the exact 3-D geometry for the DFN usually requires highly specialized expertise and a substantial amount of data including geological outcrop studies incorporating depositional and tectonic history of the area, fracture characterization studies, well logs, drilling, completion, and other field data available from the surrounding wells, in situ stress, and pore pressure/fracture gradient analysis. These extensive datasets will help to capture geomechanical properties and failure characteristics of the formation, the fluid analysis, and macro-/micro-/nanoscale geological, petrophysical and geomechanical properties. Obtaining this large dataset and associated analyses requires significant effort. Therefore, we have implemented a new approach illustrated in the workflow diagram in Fig. 8 to incorporate the needed details to obtain an effective hydraulic fracturing

operation and better reliability in the production optimization and forecasting.

### 3.1 Mechanical Earth Model with Natural Fracturing Details

The input parameters for the discrete fracture network (DFN) model needed for the integrated modeling study introduced in this study have been determined utilizing the triaxial undrained core measurements, fracture characteristics obtained from natural fracture characterization in the areas of the two core wells, the well logs, borehole imaging logs, drilling, well completion and stimulation data and analysis. The procedure has been discussed in detail in Suppachoknirun (2016).

**Fig. 6** Studied well location and the world stress map showing the maximum stress direction across the South Texas area Heidbach et al. (2008). The azimuth angle values observed from the wells in the area are in alignment with the local trends indicated on the world stress map with the red arrow at the well-pad location. Primary natural fracture orientation of N75°E and secondary fracture orientation of N20°W are used in the establishment of the DFN and later for the reservoir simulations presented in the study

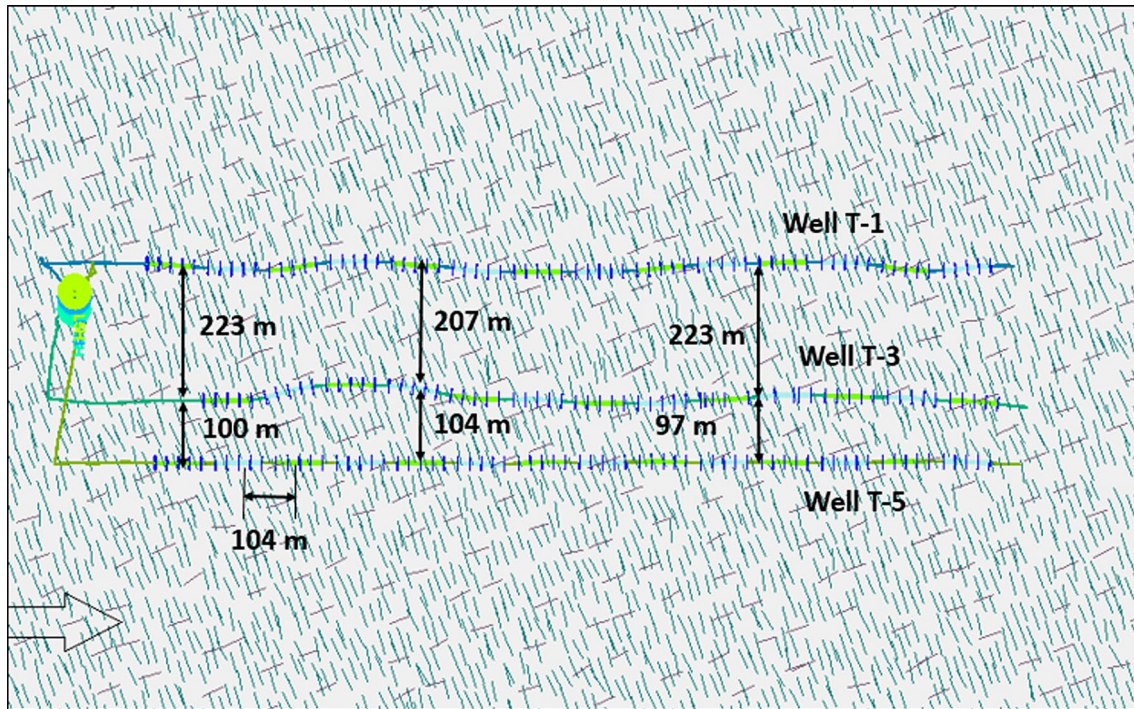
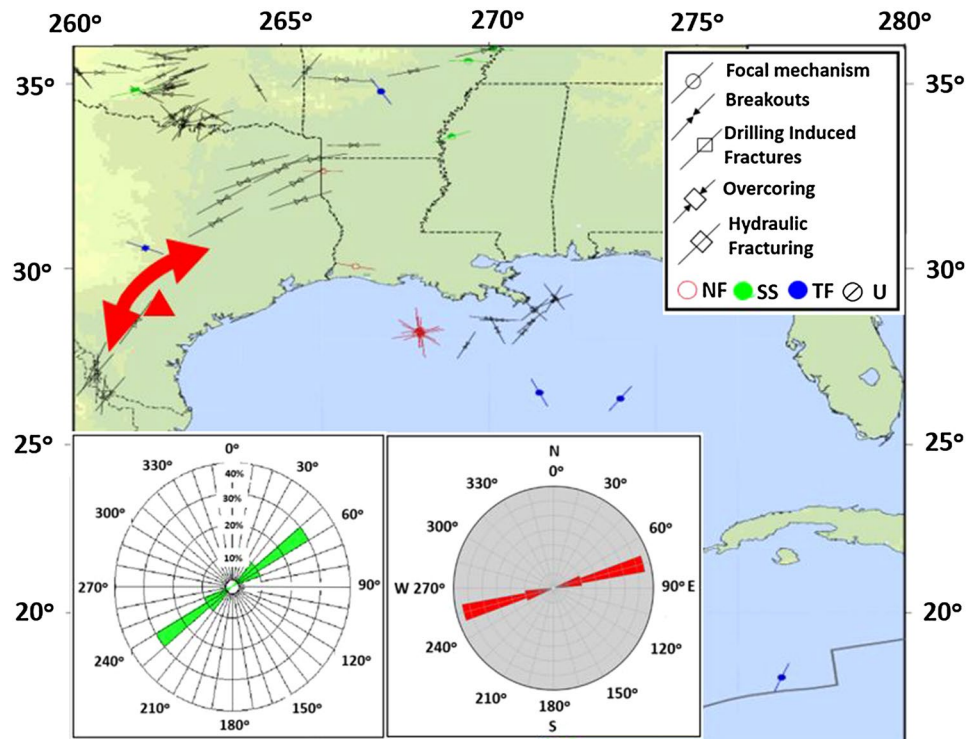


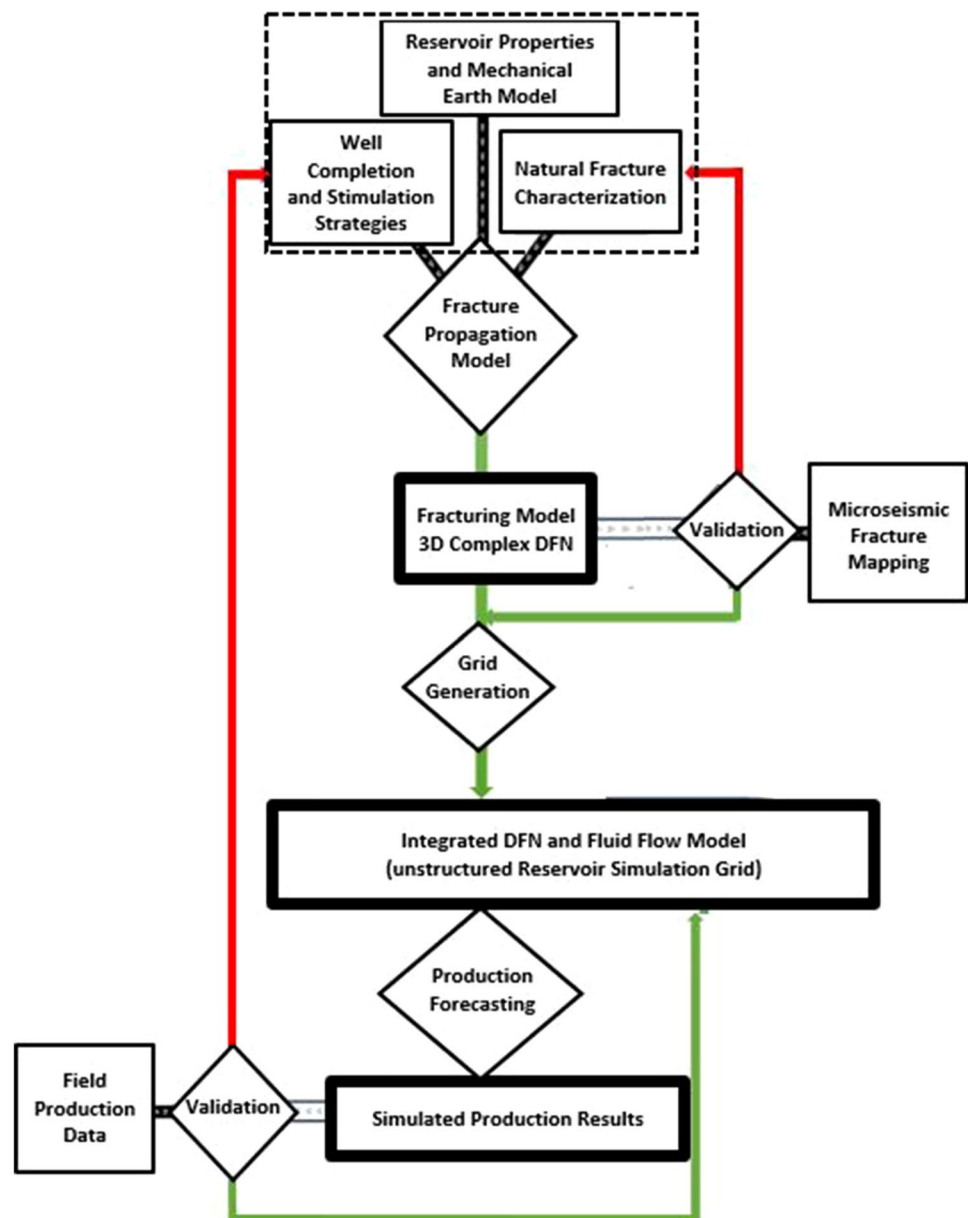
**Fig. 7** Spacing between the three horizontal wells, T-1, T-3 and T-5, natural fracture network (primary set is in green) and the hydraulic fracturing stages investigated in this research study illustrated in horizontal plane view (Suppachoknirun and Tutuncu 2016) (color figure online)

Input properties along the vertical extent and the characteristics specific to each formation include the log suites data, derived variables, or those from qualitative

interpretation. The log suite generated using the properties from the neighboring county with similar stratigraphy has also been considered as an additional source, aiding in



**Fig. 8** Workflow for the processes used in obtaining coupled DFN, hydraulic fracture and reservoir simulation model



accuracy enhancement. The maximum principal stress direction of N 75° E has been used in the model utilizing the field data presented in Fig. 6. The primary fracture azimuth was also confirmed to be in this direction from the post-job microseismic fracture mapping data.

Although the dataset needed for representing an exact 3-D DFN in the reservoir is not available because of the proprietary nature of the limited dataset released to the UNGI research consortium, a number of published studies in the Eagle Ford shale oil window in South Texas with similar stratigraphy and subsurface conditions to this study were used to obtain additional data for a reliable DFN model representative of the study area's natural fracture characteristics (Ejofodomi et al. 2015; Padin et al. 2014; Offenberger

et al. 2013; Mullen 2010). For example, Landry et al. (2014) pointed out evidence, indicating that the parallel-to-bedding natural fractures in the Eagle Ford are calcite-filled and as such are impermeable to flow until they are reactivated during the hydraulic fracturing operations. The combination of the information obtained from the UNGI wells and the published literature led to several modifications of the DFN model validated before a final DFN was obtained following the steps illustrated in Fig. 8. The geological model has been constructed as a polygon consisting of a stack of various layers dipping by 2 degrees to the horizon to represent the subsurface geology of the field from 2126 to 3267 m. true vertical depth (TVD) covering four formations from the Anachacho to the Buda. The lateral sections of the three wells

in the well-pad study area have been placed in the lower Eagle Ford as the primary target, bounded by the Austin Chalk and the Buda Limestone above and below, respectively. The 2-D and 3-D views of the geological model are shown in Fig. 9, which was used to incorporate in the DFN the interaction of the natural fractures with the hydraulic fracturing process.

### 3.2 Integrated 3-D Discrete Fracture for Hydraulic Fracturing with Natural Fracture Influence

The complex 3-D DFN was established after the hydraulic fracturing treatment to combine the natural fracture network and hydraulically induced fractures. To accomplish this modeling, the DFN model for the geological/natural fracture details has been input into the new hydraulic fracturing model to incorporate accurate fracture growth in the local conditions at the well-pad location. The technical concepts adopted in the hydraulic fracturing model are briefly summarized in this section. Further details on the modeling approach and theory implemented can be reviewed in Suppachoknirun et al. (2016) and Weng (2015).

#### 3.2.1 Governing Equations

The set of the governing equations used for numerical simulation were developed based on the fundamental laws of physics, including conservation of mass, conservation of momentum, and volumetric balance. Applications of these three conservation laws used for fracture propagation modeling are explained in detail in Weng et al. (2011) and Weng (2015). Mass conservation considers the mass balance of the fluid flow in the fracture and the fluid leaked out of the fracture into the formation. In conservation of momentum, flow rate and pressure gradient are based on the 1D fluid flow in a laminar regime along the fractures, which has

been reduced from the conservation of momentum from a 2-D flow power law without inertia effects. To satisfy the volumetric balance, the total fluid volume pumped into the system must be equal to the fluid volume within the system (fracture network including the wellbore) and fluid volume leaking out of the system.

#### 3.2.2 Fracture Width and Height

The 2-D plane-strain solution was assumed similar to that applied in the conventional pseudo-3-D model employed by Weng et al. (2011), considering the computational efficiency for the engineering design of the fracture treatment. A layered medium width average Young's Modulus has been assumed without any variability. In a multilayered formation, the height and width profiles of a fracture depend on the fluid pressure, in situ stress magnitudes, fracture toughness at the tip of the fracture, formation layer thickness, and the elastic moduli for each layer in which the fracture is contained (Mack and Warpinski 2000). Weng (2015) suggested that the fracture height can be determined at each position of the fracture by matching the stress intensity factors at the fracture tips,  $K_{Iu}$  and  $K_{II}$ , to the fracture toughness,  $K_{Ic}$ , of the corresponding layers containing the tips at the formation. The stress intensity factors at the tips were calculated as a function of the pressure in the fracture, the fracture geometry, and the formation layer stresses.

#### 3.2.3 Transportation of Fracturing Materials in Fractures

Fluid and proppant transport inside the fractures can be considered in horizontal and vertical planes, separately. In the horizontal direction, volumetric concentration calculation for a given proppant and fracturing fluid type is based on the average values over the volume from the top of the fracture to the bottom of the fracture element (Weng et al. 2011).

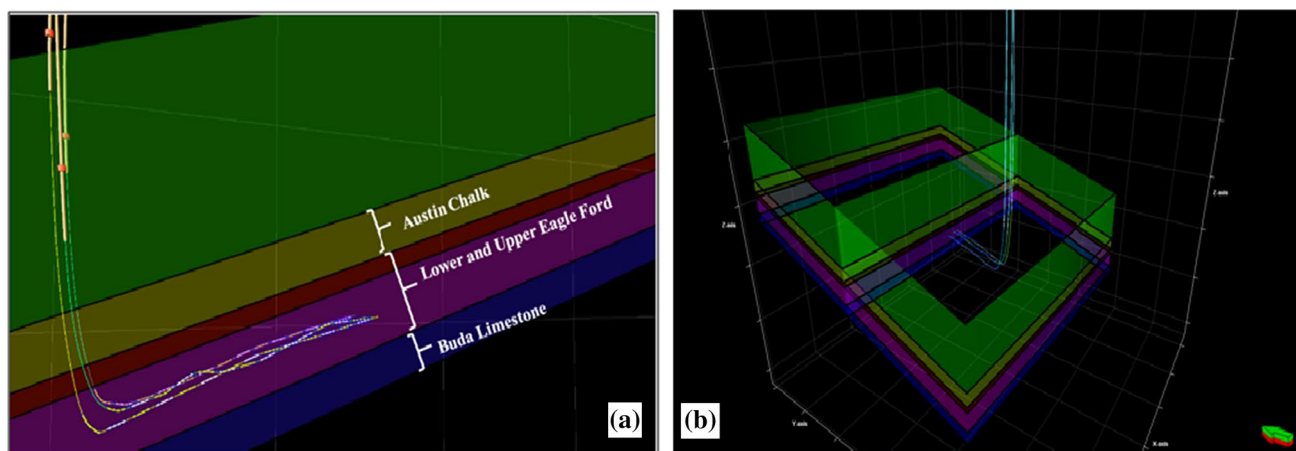


**Fig. 9** Wells and formation structural model in **a** 2-D looking west and **b** 3-D looking northeast

The proppant transportation with only advective transport in the horizontal direction has been implemented following the approach discussed in detail by Adachi et al. (2007). In the vertical direction, two major mechanisms, settling of proppant onto the bank and erosion of the existing bank, have been considered. Proppant settling velocity for a given proppant type has been computed based on the combination of the Stokes law with the drag coefficient for a spherical particle and its relationship to the Reynolds number. To consider the erosion mechanism, the erosion model by Weng et al. (2011) which specifies the minimal height of clean fluid and slurry at conditions under which the proppant does not settle and the bank is eroded, was implemented.

#### 3.2.4 Stress Shadow Effects

To account for the stress shadow effects on the fracture propagation, the effects of induced stresses from the adjacent fractures have been incorporated into the fracture network model. The displacement discontinuity method (DDM) with 2-D plane-strain assumption was used. This method has been originally introduced by Crouch and Starfield (1983) and later modified by Olson (2004).

#### 3.2.5 Interactions of Hydraulically Induced and Natural Fractures

To consider the interaction between the hydraulically induced and the natural fractures, Gu and Weng (2010) proposed an analytical method to determine whether the hydraulic fracture will cross over or be arrested by an existing natural fracture at their intersection as illustrated in Fig. 5. The interaction is affected by the principal stress ratio, hydraulic fracture approaching angle, coefficient of friction, and cohesion. When a hydraulic fracture is approaching an existing natural fracture, the hydraulic fracture will propagate across the existing fracture (i.e., a new fracture is created on the opposite side of the interface), provided that the maximum principal stress is not less than the rock tensile strength. In other words, the stress acting on the fracture surface is able to transmit its tip stress across the interface to create the fracture on the other side of the natural fracture. To satisfy this condition, the stress acting on the interface must not cause slip at the interface. This no-slip condition at the interface for a frictional rock can be represented using the relationship of stresses acting at the interface. The total stress acting on the interface is the combination of the two remote principal stresses and the fracture tip stress.

#### 3.2.6 Reservoir Simulation and Validation

Fracture simulation has been conducted based on the field data collected during the fracturing treatment. A delayed

borate-cross-link fluid system utilizing hydroxypropyl guar (HPG) gelling agent was used as the fracturing fluid. Premium white sand with three different sizes, 40/70, 30/50, and 20/40, was used as the proppant. After pumping the pad, slurry was pumped into the well in multiple pumping stages with gradually increasing proppant concentration in 0.06 kg/L increments to a maximum concentration of 0.42 kg/L.

Microseismic data have been utilized for the validation of the complex DFN model developed as shown for the two of the wells in Fig. 10. The unified complex discrete fracture network used as the input for the reservoir simulation for production forecasting is illustrated in 2-D and 3-D as shown in Fig. 11. The associated stimulated reservoir area obtained from the hydraulic fracturing operation is presented in Fig. 12.

### 3.3 Reservoir Modeling for Production Prediction

Initial production forecast was conducted using zipper fracturing geometry in the well pad as it was the chosen design applied in the field. Unstructured production grid blocks with three different fracture geometries were introduced using the original natural fracture DFN. Then, the obtained complex fracture network was used to production forecasting. The validations of both the complex fracture model and fluid flow simulation model have been conducted using the field data collected at the well pad.

The concepts of black oil fluid model have been applied. Production logs were utilized for obtaining the reservoir fluid properties. The formation volume factor, fluid, and viscosity of each phase have been determined from the relations at a particular condition during the production simulation. Water is considered as the wetting phase of the rock matrix; hence, the relative permeability functions used for three-phase fluid flow calculations have been derived based on two sets of Corey's correlations having two mobile fluids at a time (i.e., oil–water and gas water systems). Saturation-weighted interpolation using the Baker's correlation (Baker 1988) was then utilized to develop relative permeability for three-phase fluid flow. Derivation of the relative permeability model for fluid flow in the proppant-filled fractures fluid was based on smaller Corey's exponents than those considered for matrix, resulting in higher relative permeability in the fracture than in the matrix, generally experienced in most circumstances. The input dataset has been validated ensuring realistic representative behaviors of those expressed in the formation as summarized in Table 1.

The simulation grid used in the integrated fracture and fluid flow model consists of 4,439,320 grid cells and is shown in Fig. 13a. Variable shapes and sizes of the grid

**Fig. 10** Well T-1 in stages 9–11 (in orange box), and well T-5 in stages 12–13 (in red box) indicate good agreement between local fracture orientations of the complex fracture network created in the DFN modeling study and the microseismics fracture mapping obtained in the field during the hydraulic fracturing operation (color figure online)

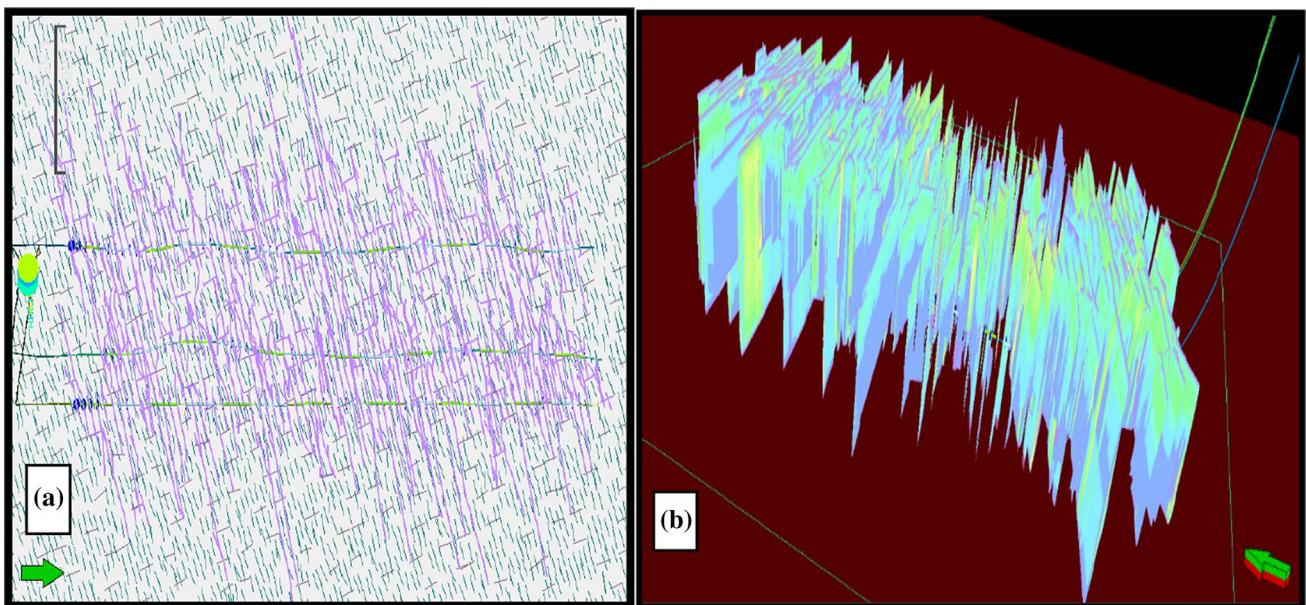
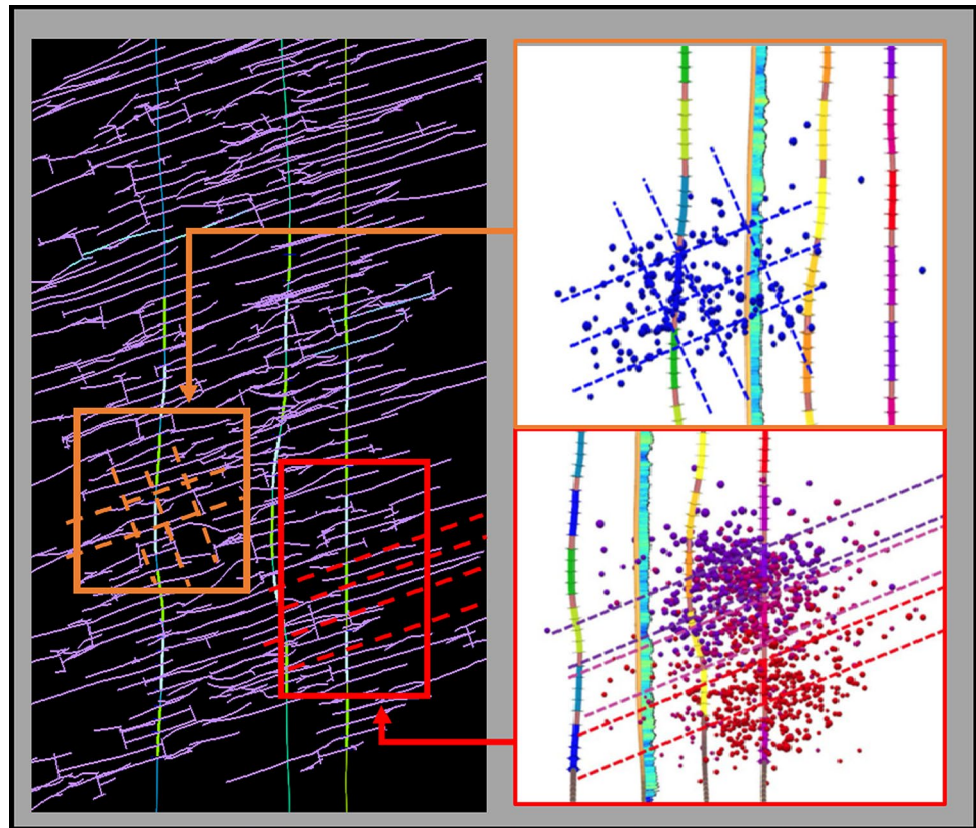


**Fig. 11** Complex coupled natural and hydraulic fractures are illustrated in the integrated DFN built **a** in 2-D plane view and **b** in 3-D

blocks have been used. Smaller cell sizes were utilized in the matrix and near the tip of the fractures as well as at the perforation areas while further away from the fractured

areas, large cells were employed. The resolution of the cells used in the simulations will have an effect on the fracture conductivities calculated. The vertical layering refinement

**Fig. 12** Stimulated reservoir area (SRA) of the complex fracture network from the model simulation of hydraulic fracturing in the Eagle Ford oil window well pad used for the study (Suppachoknirun 2016)

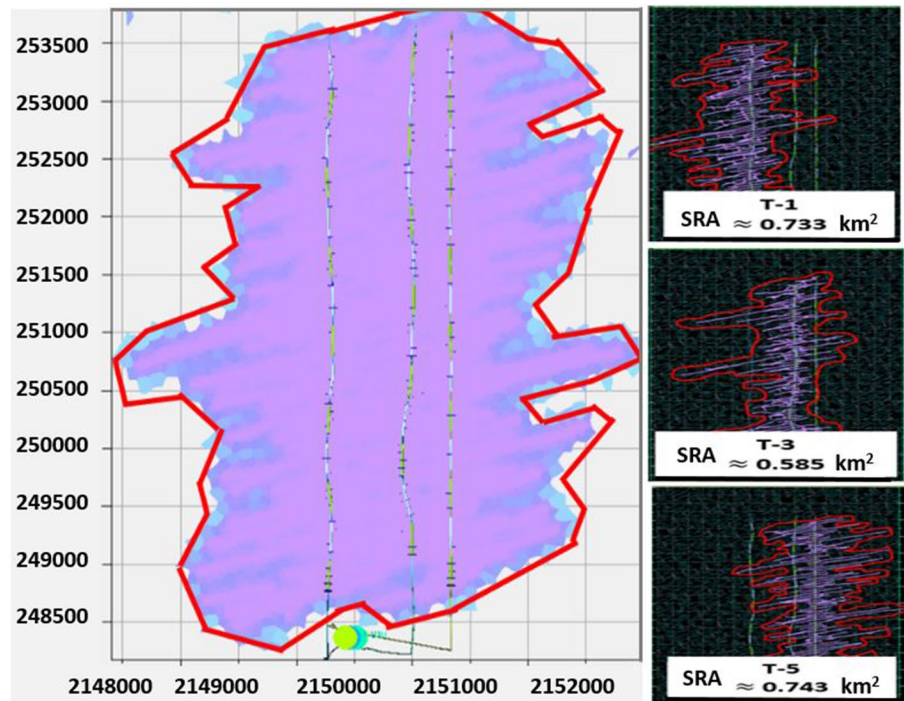


**Table 1** Input parameters obtained from the field data and complex DFN model established for the production performance and forecast

Reservoir depth (m. TVD)	3292–3350	Gas gravity	0.78
Formation dip (degree)	2.0	Oil API gravity	41
Reservoir temperature (°C)	122	Solution gas–oil ratio (SCF/STB)	1500
Overburden stress (MPa)	79–81	Bubble point pressure (MPa)	29.15
Initial reservoir pressure (MPa)	60–61	Water salinity (ppm)	15,000
Maximum stress orientation	N 75°E	Water viscosity (cp)	0.376
Young’s modulus (MPa)	182–185	Water formation volume factor (RB/STB)	1.025
Poisson’s ratio	0.25–0.26	Water compressibility (MPa <sup>-1</sup> )	4.35 E–4
Rock compressibility (MPa <sup>-1</sup> )	2.9 E–4	Initial oil saturation (%)	70
Biot coefficient	0.95	Elevation to reference (m)	108.5
Primary NF ave. L (m)	38	KOP (m. TVD)	3139–3170
Primary NF ave. spacing (m)	15.25	Total perforation interval (m)	1524–1829
Secondary NF Ave. L (m)	61	Lateral section: inclination (degrees)	92–92
Min. induced fracture perm (mD)	0.0015	Lateral section: orientation	N–S
Max. induced fracture perm (D)	27,392	Number of stages (T1, T3, T5)	14, 13, 14
Ave induced fracture perm (D)	12.03	Perforation per stages	5
Unpropped fracture. conductivity (mD-m)	3.05E–4	Distance between the adjacent stages (m)	24.4
Matrix permeability (mD)	0.0003	Perforation spacing (m)	19.5 20.1
Max. fracture conductivity (mD-m)	914	Collapse–burst resistance (MPa)	121–110.9
Average fracture conductivity (mD-m)	9.6	Perforation interval (single) (m @ 4 SPF)	0.81
Tensile strength (MPa)	2.7–6.1	Perforation diameter (cm)	5.08
Friction coefficient	0.6		

Total production grids 221,966 × 20 (4,439,320 cells) for (ij × k) were used

has been implemented based on the local property variations to incorporate the heterogeneity. In order to conduct the production optimization, a smaller model shown in Fig. 13b was

established for the fracturing stages 9, 10, and 11 of all three wells in the pad. Then, the total production from the smaller model was normalized to the full model.

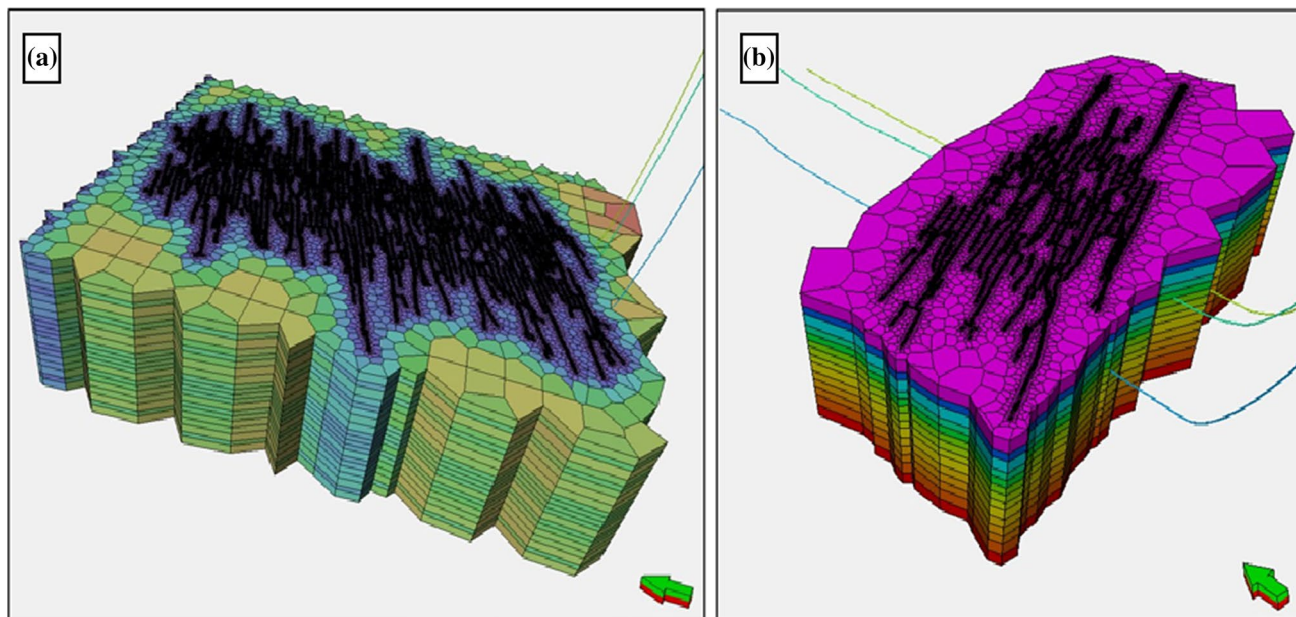


**Fig. 13** **a** Production grid created based on 3-D complex coupled fracture network. **b** A smaller production grid from stages 9, 10, and 11 in the three wells in the pad was used for the optimization study

#### 4 Production Optimization Using Three Different Fracture Geometries in the Eagle Ford Formation

Historical production data from the field for a period of 15 months after the hydraulic fracturing operation in the three wells have been used to validate the hydraulic fracturing and production model using zipper fracturing geometry. A good agreement to the field oil and gas production

and cumulative productions was obtained as presented in Suppachoknirun and Tutuncu (2016). Significant pressure change first occurred in the area with highly complex fractures before slow distribution into the less-complex fracture region and matrix region as shown in Fig. 14.

A similar analysis using the original natural fracture DFN as an input has been conducted to simulate hydraulic fracturing of the formation using alternating fracturing and consecutive fracturing patterns and running the reservoir

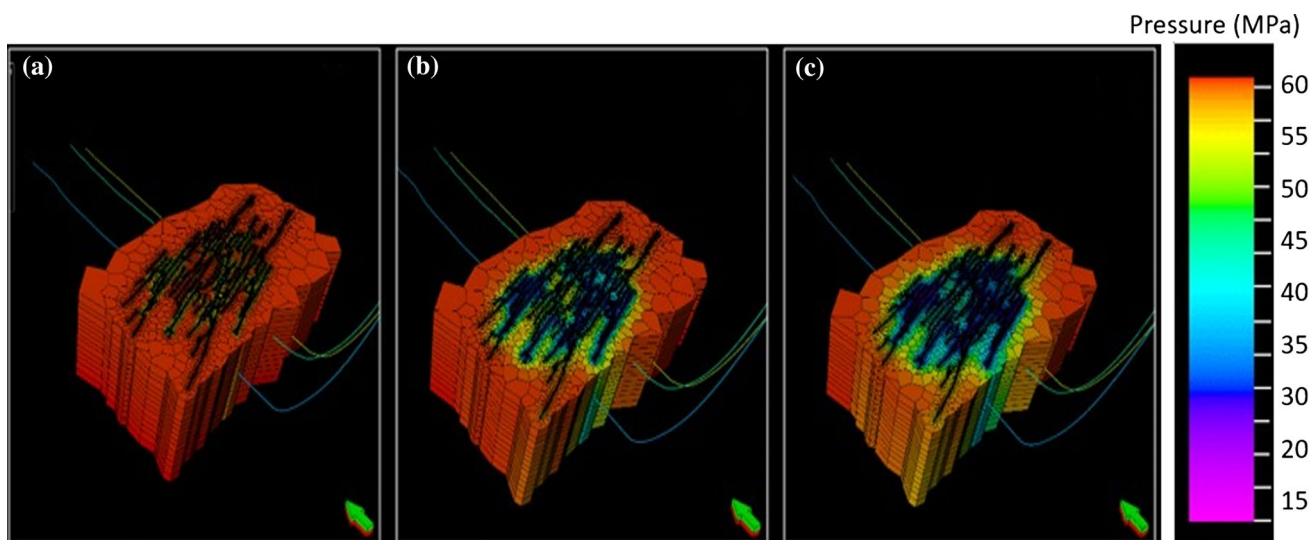


**Fig. 14** Pressure distribution in the Eagle Ford well pad using zipper fracturing geometry after the wells have been producing **a** the first day, **b** 1 year after the fracturing, and **c** 2 years

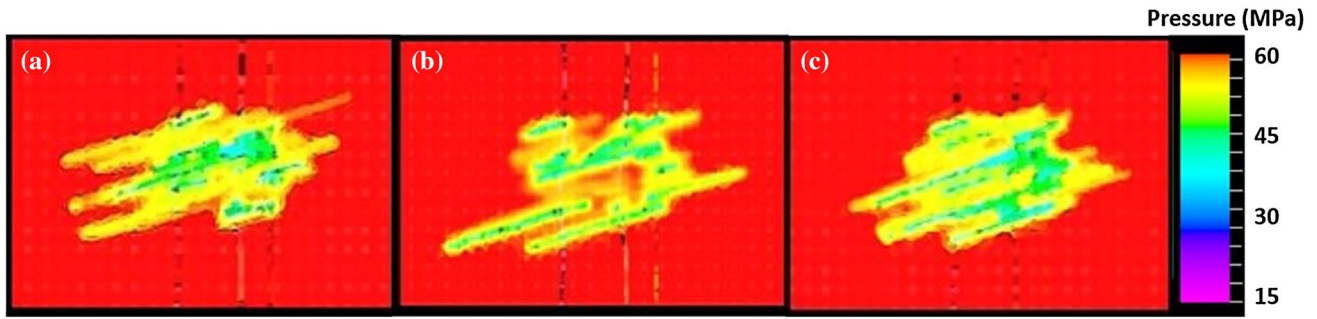
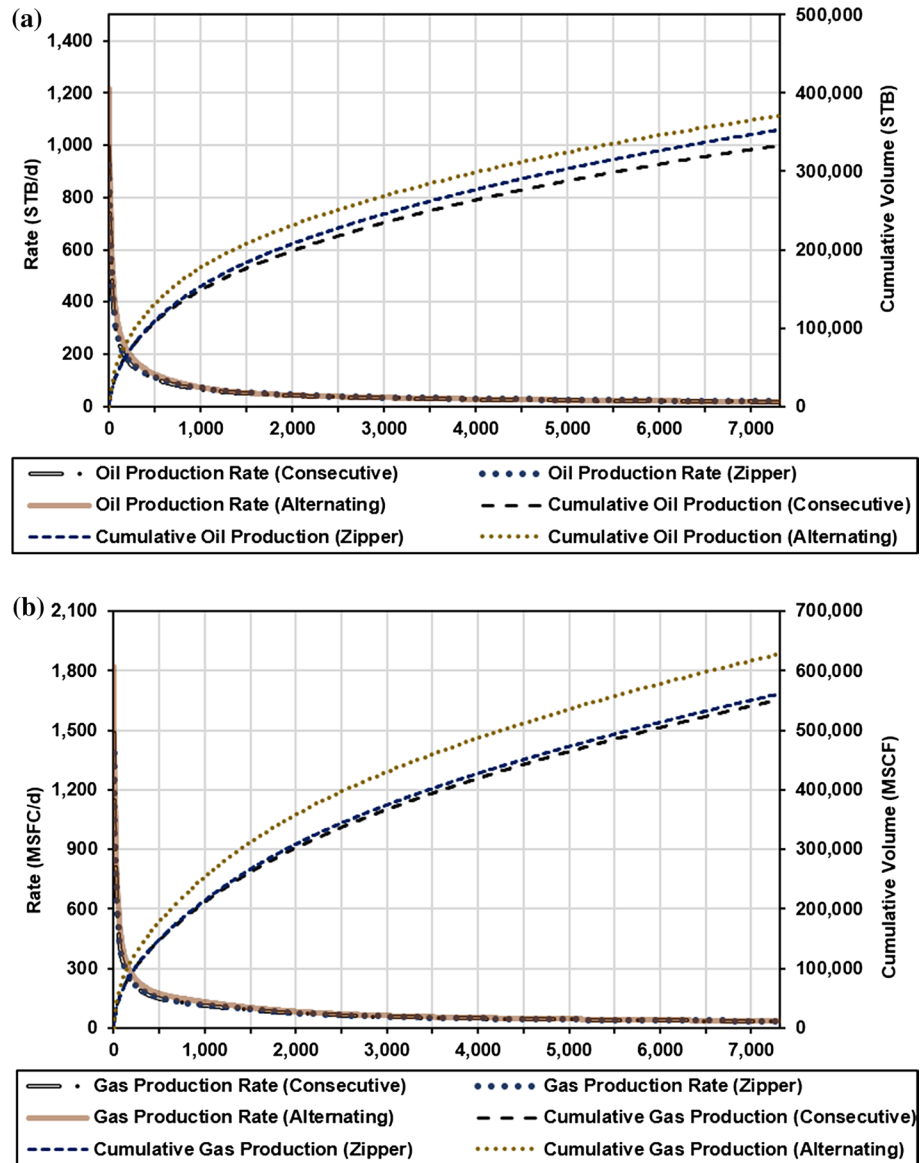


**Fig. 15** Pressure variations in the well pad in the one-year production period: **a** consecutive fracturing **b** zipper fracturing **c** alternating fracturing

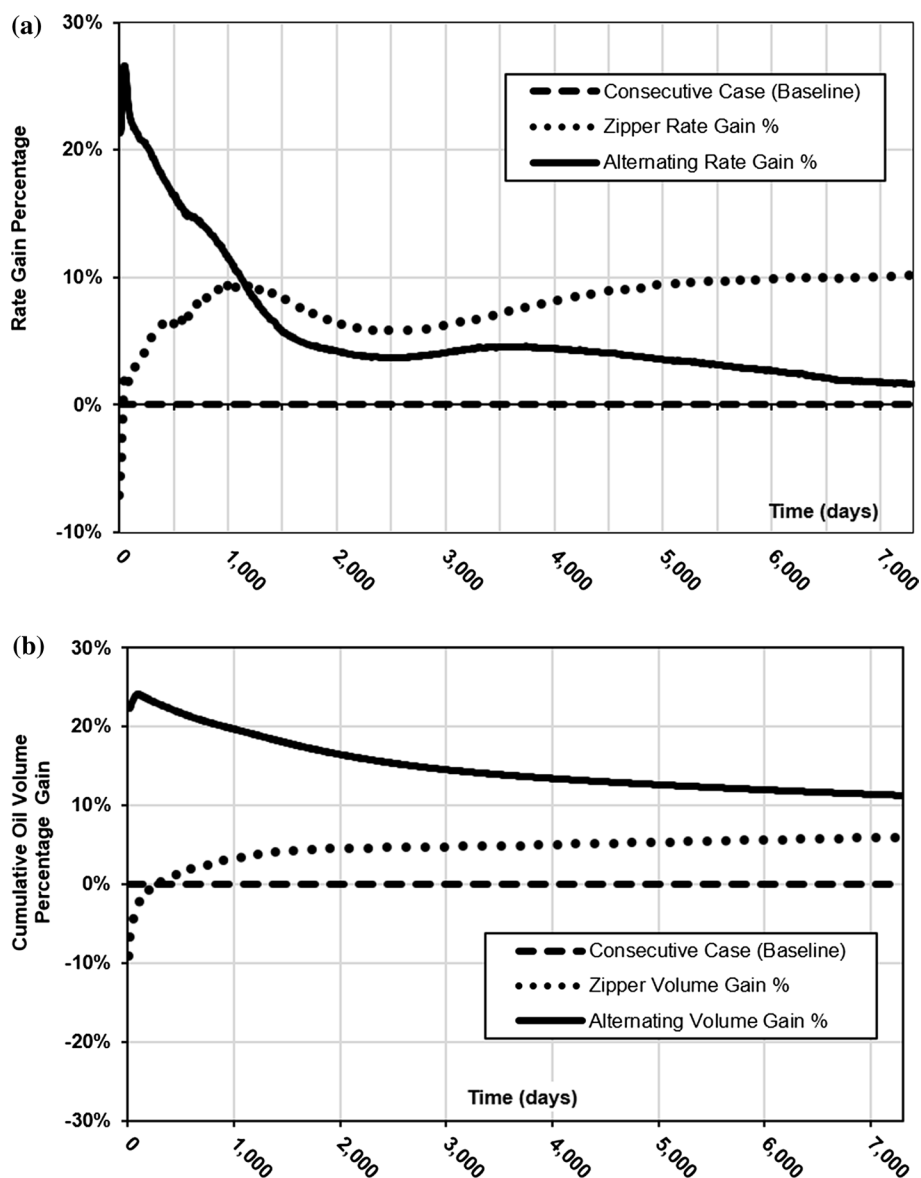
**Fig. 16** Production rates and cumulative production in the Eagle Ford oil window well pad using zipper, consecutive and alternating fracture patterns. **a** Oil production rate and cumulative oil production as a function of time for 20 years, **b** gas production rate and cumulative gas production as a function of time for 20 years



simulator for production in the same well pad. The pressure variations for the three fracturing processes in the same well pad are compared in Fig. 15. The production rate and

cumulative volume of oil and gas over 20 years of continuous production are presented in Fig. 16. The additional production rates and cumulative production gained from zipper

**Fig. 17** Comparison for zipper, consecutive and alternate fracturing geometries relative to the consecutive fracturing case: **a** production rate change and **b** cumulative oil volume change



and alternating patterns are compared to consecutive fracturing in Fig. 17. The contribution to production from each well toward the cumulative production was shown to be unequal. The T-1 well contributes significantly to overall production, 47.4 and 42.8% in the alternating fracturing case and zipper fracturing case, respectively, and more than 50% in the consecutive fracturing case. On the contrary, the T-3 well contributes least to the produced volume at the pad in most circumstances based on the simulation results. These results can be linked to the portion of the fractures created from the hydraulically induced fractures initiated in each well in the full unified complex fracture network. Well location and the spacing between the wells are among the main parameters contributing the unequal production.

### 5 Conclusions

A new coupled geomechanics and fluid flow model using detailed natural fracture information in the study area and incorporating the interaction between the natural fractures and the hydraulic fracture during the propagation of the hydraulic fracture have been introduced for reliable forecasting of the hydraulic fracturing process and production. The new approach and the coupled model have been utilized in three horizontal wells in an Eagle Ford oil window well pad. Three different fracturing scenarios have been modeled to have three different hydraulic fracture geometries representing the role of hydraulic fracturing pattern on the produced oil and gas at the same well pad. Coupling geomechanics



and flow in the model and incorporating reservoir properties obtained from the core measurements and well logging, fracturing and microseismic data provided significant variation in the production forecast for different fracture geometries. In contrast to the conventional hydraulic fracturing models with symmetric bi-wing planar hydraulic fracture in the reservoir, non-planar fractures have been obtained with the embedment of the DFN model concerning the natural fractures and the hydraulic fracturing.

It is evident from the results presented in this study that the interactions of hydraulically induced and preexisting fractures, hydraulic fracture propagation mechanics, proppant transport, stress shadowing effects, and the operational parameters are essential to include in any modeling effort for reliable production forecast. The production from each well is not typically measured. Instead, the commingled production rate is recorded. This could give erroneous results as the contribution of each well, particularly in the early phase of the production, is different.

According to the simulated production results using the approach and strategy adopted in the research study presented here, the pad with the alternating fracturing technique produces more oil than with zipper fracturing in a 20-year production period. A significant drop in the production rate within the first few years could be anticipated in a shale reservoir regardless of the fracturing technique implemented. The initial oil rate in the alternating fracturing case could be greater than for the zipper fracturing until a specific period of time after which zipper fracturing has the lowest decline rate among the three cases considered. Although the alternating fracturing technique provides relatively higher production volumes than the other patterns, its implementation in the field might not be easy with the current technologies used in hydraulic fracturing. The zipper fracturing pattern might not produce the highest volume over the 20-year period based on the analysis results obtained in this study. The differences in cumulative production between these two patterns become less over time. From an operational perspective, field application of the zipper fracturing technique appears to be more practical and has been widely used in various shale reservoirs. Since the implementation sequence of the zipper fracturing technique allows the operation to be simultaneously carried out on multiple wells, this process requires less time and associated cost.

The stimulated reservoir volume and production from any tight reservoir can be obtained using the coupled model presented in this study. Accuracy and realistic representation of the stimulated reservoir volume and production can be enhanced by incorporating natural fractures and a full 3-D reservoir model with realistic anisotropy and heterogeneity utilizing field and core data.

**Acknowledgements** The authors would like to thank the Unconventional Natural Gas and Oil Institute (UNGI) in Colorado School of Mines for the research opportunities; UNGI CIMMM Consortium members for the field data used and the project sponsorship; and PTT Exploration and Production Plc. for their support during the first author's graduate studies at Mines.

## References

- Adachi J, Siebrits E, Peirce A (2007) Computer simulation of hydraulic fractures. *Int J Rock Mech Min Sci* 44(5):739–757
- Baker LE (1988) Three-phase relative permeability correlations. In: *Proceedings of SPE enhanced oil recovery symposium*, Tulsa, Oklahoma, 16–21 April. SPE-17369
- Crouch SL, Starfield AM (1983) *Boundary element methods in solid mechanics: with applications in rock mechanics and geological engineering*, 1st edn. George Allen & Unwin, London
- Donovan AD, Staerker ST (2010) Sequence stratigraphy of the Eagle Ford (Boquillas) formation in the subsurface of South Texas and Outcrops of West Texas: *Transactions—Gulf Coast Association of Geological Societies*, 60, 861–899
- Ejofodomi EA, Baihly JD, Silva F (2015) Using a calibrated 3D fracturing simulator to optimize completions of future wells in the eagle ford shale. In: *SPE-178680. Proceedings of unconventional resources technology conference*
- Gu H, Weng X (2010) Criterion for fractures crossing frictional interfaces at non-orthogonal angles. ARMA-10-198. In: *Proceedings of 44th US rock mechanics symposium and 5th US–Canada*
- Heidbach O, Tingay M, Barth A, Reinecker J, Kurfeß D, Müller B (2008) *The World Stress Map database release 2008*. <http://doi.org/10.1594/GFZ.WSM.Rel2008.2008>
- Landry C, Eichhubl P, Prodanovic M, Tokan-Lawal A (2014) Matrix-fracture connectivity in Eagle Ford shale. In: *SPE-1922708. Proceedings of unconventional resources technology conference*
- Mack MG, Warpinski NR (2000) *Mechanics of hydraulic fracturing*. In: Economides S, Nolte K (eds) *Reservoir stimulation*, 3rd edn. Wiley, London
- Martin R, Baihly J, Mulpani R, Lindsay GJ, Atwood WK (2011) Understanding production from Eagle Ford–Austin Chalk system. In: *SPE-145117. Proceedings of SPE annual technical conference and exhibition*
- Mokhtari M, Tutuncu AN (2016) Impact of laminations and natural fractures on rock failure in Brazilian experiments: a case study on green river and Niobrara formations. *J Nat Gas Sci Eng* 36:79–86
- Mokhtari M, Bui BT, Tutuncu AN (2014) Tensile failure of shales: impacts of layering and natural fractures. In: *SPE-169520. Proceedings of SPE Western North American and Rocky Mountain Joint Meeting*
- Mullen J (2010) Petrophysical characterization of the Eagle Ford Shale in South Texas. In: *Proceedings of Canadian unconventional resources and international petroleum conference*, Calgary, Alberta, Canada, 19–21 October. SPE-138145-MS
- Offenberger R, Ball N, Kanneganti K, Oussoltsev D (2013) Integration of natural and hydraulic fracture network modeling with reservoir simulation for an Eagle Ford well. In: *SPE-168683. Proceedings of unconventional resources technology conference*
- Olson JE (2004) Predicting fracture swarms—The influence of subcritical crack growth and the crack-tip process on joint spacing in rock. *Geol Soc Spec Publ* 231:73–87
- Padin A, Tutuncu AN, Sonnenberg S (2014) On the mechanisms of shale microfracture propagation. In: *SPE-168624. Proceedings of SPE hydraulic fracturing technology conference*

- Padin AD, Ramiro-Ramirez S, Sonnenberg S, Tutuncu AN (2016) Morphology of organic-rich shale and implications for the development of microfractures during hydraulic fracturing. In: Proceedings of 78th EAGE conference and exhibition, Barcelona, Spain
- Rafiee M, Soliman MY, Pirayesh E (2012) Hydraulic fracturing design and optimization: a modification to zipper frac. In: SPE-159786. Proceedings of SPE annual technical conference and exhibition
- Robinson CR (1997) Hydrocarbon source rock variability within the Austin chalk and Eagle Ford shale (upper cretaceous), East Texas, USA. *Int J Coal Geol* 34:287–305
- Roussel NP, Sharma MM (2011) Optimizing fracture spacing and sequencing in horizontal-well fracturing. *SPE Prod Oper* 26(2):173–184
- Suppachoknirun T (2016) Evaluation of multi-stage hydraulic fracturing techniques to optimize production in naturally fractured reservoirs using a DFN-based numerical technique, MS Thesis, Colorado School of Mines, Golden, Colorado
- Suppachoknirun T, Tutuncu AN (2016) Evaluation of multistage hydraulic fracture patterns in naturally fractured tight oil formations utilizing a coupled geomechanics-fluid flow model—case study for an Eagle Ford shale well pad. In: Proceedings of, 50th US rock mechanics/geomechanics symposium, Houston, Texas, 26–29 June, ARMA-16-782
- Suppachoknirun T, Tutuncu AN, Kazemi H (2016) Evaluation of multistage hydraulic fracturing techniques for production optimization in naturally fractured reservoirs using coupled geomechanics fracture and flow model. In: IPTC-18916. Proceedings of international petroleum technology conference
- Tutuncu AN (2015) An experimental and modelling study for geomechanical and flow characteristics of Eagle Ford and Vaca Muerta Shale formations. In: Proceedings of Houston Geological Society Applied Geoscience Conference, Geomechanics in Unconventionals
- Tutuncu AN (2017) Hydraulic fracturing fundamentals, chap. 2 in hydraulic fracturing law and practice, 2017 Edition, LexisNexis, ISBN: 9781632838988
- Tutuncu AN, Katsuki D, Padin A, Bui B, McDowell B (2016) Coupling geomechanics and petrophysical measurements for production enhancement in organic-rich shales. In: SPE 2461986, proceedings of unconventional resources technology conference, San Antonio, Texas
- US Energy Information Administration (2014) Updates to the EIA Eagle Ford Play Maps Report. Dec 2014
- Waters GA, Dean BK, Downie RC, Kerrihard KJ, Austbo L, McPherson B (2009). Simultaneous hydraulic fracturing of adjacent horizontal wells in the woodford Shale. In: SPE-119635. Proceedings of SPE hydraulic fracturing technology conference
- Weng X (2015) Modeling of complex hydraulic fractures in naturally fractured formation. *J Unconv Oil Gas Resour* 9(1):114–135
- Weng X, Kresse O, Cohen E, Wu R, Wu H (2011) Modeling of hydraulic-fracture-network propagation in a naturally fractured formation. *SPE Prod Oper* 26(4):368–380